Sensors & Actuators: B. Chemical 286 (2019) 600–607

Contents lists available at ScienceDirect

Sensors and Actuators B: Chemical

journal homepage: www.elsevier.com/locate/snb

Metasurface based on cross-shaped plasmonic nanoantennas as chemical sensor for surface-enhanced infrared absorption spectroscopy

Valentina Di Meo[a,1,2], Andrea Caporale[b,2], Alessio Crescitelli[a], Mohammed Janneh[c], Elia Palange[c], Andrea De Marcellis[c], Marianna Portaccio[d], Maria Lepore[d], Ivo Rendina[a], Menotti Ruvo[b], Emanuela Esposito[a,*]

[a] Institute for Microelectronics and Microsystems, National Research Council, I-80131 Naples, Italy
[b] Institute of Biostructure and Bioimaging, National Research Council, I-80134 Naples, Italy
[c] Department of Industrial and Information Engineering and Economics, University of L'Aquila, I-67100, Italy
[d] Department of Experimental Medicine – University of Campania "L. Vanvitelli, I-80138 Naples, Italy

ARTICLE INFO

Keywords:
Label-free detection
Surface-Enhanced InfraRed Absorption (SEIRA)
Metasurface
Plasmonic nanoantennas
Localized surface plasmon resonances
Nanotechnology

ABSTRACT

Infrared spectroscopy is an effective technique extensively used in research and industry for the label-free and unambiguous identification of molecular species. However, the sensitivity of this technique is severely limited as a result of Beer's law and, the small infrared absorption cross-section that make prohibitively weak the absorption signals, of minute amounts of analyte as those present in monolayers. This limitation can be overcome by enhancing the infrared vibration of molecules through the enhancement of the electromagnetic (EM) field. Surface Enhanced InfraRed Absorption (SEIRA) using resonant metal Nano-scale Antennas (NAs) can provide huge electromagnetic fields on the nanometer scale featuring localized collective oscillations of electrons, an effect named Localized Surface Plasmonic Resonances (LSPRsWe here report on a series of 2D arrays of cross-shaped NAs having several mm^2 area coverage (metasurface) as SEIRA optimized antennas, which can be used in practical applications such as the vibrational sensing of chemical and biological analytes. Cross-shape designed NAs are insensitive to the polarization of the electromagnetic radiation impinging the active area. Due to the random orientation of the dipole moments of molecules they are particularly suitable for the construction of biomolecular sensors. At the same time, the 2D-array configuration ensures a good near-field signal enhancement arising from the coupling between neighbour NAs Moreover, SEIRA NAs can be easily integrated with micrometre-sized channels and be suitable for the high sensitivity, real time analysis of IR emitting samples, in matrices where IR spectroscopy is severely limited due to absorption bands of liquid water. We present the design, fabrication and experimental characterization of large-area metasurfaces based on cross-shaped plasmonic NAs for the spectroscopic characterization of various types of compounds and for sensing applications in the mid-infrared range. The cross-shaped NAs we have designed exhibit SEIRA phenomena which are very sensitive to both refractive index changes in the surrounding medium and to the specific molecular vibration band emerging from surface adsorbed molecules. To test this effect on our device, we have used as model compounds small molecules (molecular weight (MW) < 500 g/mol) containing triple bond groups resonating at about 2100 cm^{-1} and a large polymer (MW ˜ 950,000 g/mol) containing carbonyl groups resonating at wavenumbers of about 1700 cm^{-1}. We show a sensitivity of 600 nm/*RIU* at different wavelengths at a maximum amount of immobilized small molecule of 0.7 fmoles and a SEIRA enhancement factor of 48,000. We also show the device potential to reveal chemical reactions, occurring on the sensor surface at the same scale, where the nitrile group is converted to a triazole ring.

* Corresponding author.
E-mail address: emanuela.esposito@cnr.it (E. Esposito).
[1] University of Calabria, I-87036 Rende, Italy.
[2] These authors contributed equally to this work.

https://doi.org/10.1016/j.snb.2019.02.014
Received 28 June 2018; Received in revised form 27 December 2018; Accepted 3 February 2019
Available online 04 February 2019
0925-4005/ © 2019 Elsevier B.V. All rights reserved.

1. Introduction

Infrared (IR) spectroscopy provide direct information on functional groups occurring in a molecule via their own characteristic absorption spectrum in a univocal, non-destructive and label-free way. It is a useful technique complementary to other analytical methods. The different spectroscopic techniques, like rotational spectroscopy, nuclear magnetic resonance spectroscopy, ultra violet spectroscopy and mass spectrometry each contributes to the knowledge of the "system" analyzed by providing complementary information. Of great practical interest for the analysis of organic and biological molecules, is the spectral area between 4000 and 400 cm^{-1}. IR radiation between 10.000 and 100 cm^{-1} is absorbed from organic molecules and converted to vibrational motion energy. This absorption is quantized, but vibrational spectra appear as bands rather than as lines because of the change in vibrational energy accompanied by variations in the rotational state. The bands are in fact roto-vibrational bands. There are two important areas for a prompt examination of an IR spectrum: the region between 4000 and 1300 cm^{-1} and that between 1300 and 900 cm^{-1}. The high frequency region is called region of functional groups. Absence of absorption in the ranges assigned to the various functional groups indicates the absence of such groups in the molecule. The intermediate region of the spectrum at 1300-900 cm^{-1} is generally referred to as the fingerprint region since absorption bands here may represent a unique signature for each molecule [1]. Thanks to its fast and routine use for the structural investigation of chemical compounds Fourier Transform InfraRed (FTIR) spectroscopy is widely employed in various fields of research, in industry as well as in pharmaceutical, safety, food, and forensic sciences to identify substances [2,3]. Moreover, in health can be used to tissue classification and cancer identification (trough hyperspectral imaging).

Infrared spectroscopy is characterized by a very low molecular absorption cross-section of infrared vibrations ($\sigma_{abs} \approx 10^{-20}\,cm^2$); therefore, a large amount of material is necessary for accurate determinations. Accordingly, the spectroscopic characterization of minute amounts of analytes, like self-assembled monolayers, required for sensing applications, is not practical, since extremely weak signals are expected based on Beer's Law predictions. This fundamental limitation can be overcome by the use of metallic nanoantennas (NAs) that support Localized Surface Plasmonic Resonances (LSPRs).

Metal NAs having sub-wavelength size (dimension smaller than the wavelength of the incident electromagnetic radiation) can be seen as oscillators, whose behavior is determined by the effective mass, by the charge and density of free electrons and by their geometry. Under resonance conditions, the electric dipoles induced inside each nanostructure become extremely large. Consequently, the local fields in proximity of the particles are enhanced compared to the incident fields, so the absorption cross-section can be greatly amplified, and strong absorption peaks are observed. These collective excitations are known as Localized Surface Plasmons Resonances. These modes strongly depend on the particle size (relative to the incident wavelength), on the shape and on the environment in which the nanostuctures are located. [4–7]. LSPRs can originate phenomena of Surface Enhanced Infrared Absorption (SEIRA).

Metal NAs arranged in a 2D-array geometry, i.e. metasurfaces, are generally deposited on a dielectric or semiconductor substrate. In principle, depending on the specific application, the optical response of the metasurfaces can be tailored in any region of the electromagnetic spectrum from visible to microwave by varying the periodicity of the 2D-array as well as the shape, size and metal film thickness of each NA [8,9]. For spectroscopic and sensing applications in the infrared range, highly efficient sensing devices can be designed exploiting the significant enhancement of IR signal in well-defined infrared regions [10]. In particular, it is possible to increase the sensitivity in the detection of chemical and biological substances when two 2D-arrays of plasmonic nanoantennas are used in SEIRA spectroscopy [11–13]. The condition needed by metasurfaces to probe the presence of chemical and biological substances adsorbed on their surface is the accordance between the plasmonic resonance of the functionalized NAs and the wavelength value at the maximum absorption of the substance [11,12]. In these conditions, the value of the metasurface reflection coefficient is modified, allowing the identification of the adsorbed species. The resonance wavelength scales linearly with antenna's length (L) and with the refractive index (RI) of the surrounding medium [14]. Such dependence on the antenna's geometrical parameters offers the possibility to tailor an optimized design of the NAs and, through nanofabrication technologies, to realize metasurfaces with the desired resonance wavelength. Theoretical and experimental investigations have focused the attention on understanding how variations of the shape and/or the geometrical parameters characterizing both the NAs and the resulting 2D-array influence the SEIRA detection sensitivity. Several types of NAs, different in shape, size, geometrical parameters and thickness [15–19] have been proposed in order to explore their influence on the metasurface detection sensitivity. The variation of only one of these parameters results in a shift of the peak wavelength λ_{res} of the metasurface reflection/transmission curve and, in changes of the maximum achievable reflection coefficient and of the bandwidth measured at full width at half maximum.

In this paper we present the design, fabrication and experimental characterization of large-area coverage arrays of cross-shaped plasmonic NAs for vibrational sensing in the mid-infrared range. The cross-shaped design makes NAs insensitive to the polarization of the electromagnetic radiation impinging the active area. This feature enables their utilization as bio-molecular sensors, given the random orientation of the dipole moments of molecules. At the same time the array arrangement ensures a good near-field signal enhancement arising from the coupling between neighbour NAs. The combined collective and individual plasmonic responses of the 2D array of NAs play a crucial role to obtain signal enhancement factors of 10^4–10^5. Although cross-shaped 2D-arrays of NAs have been reported as refractive index sensors [20,21], their ability as detectors of the SEIRA resonant effect has not been reported so far.

Enabled by the high quality, precision and reproducibility of the Electron Beam Lithography technique in terms of arrangement of nanostructures, we have manufactured very homogeneous, robust and recyclable arrays using float-zone silicon wafer as substrates. The generated cross-shaped NAs exhibit SEIRA phenomena which are very sensitive to both refractive index changes in the surrounding medium and, to the specific molecular vibration band emerging from surface adsorbed molecules. Acting on the 2D array geometrical parameters we have designed two sets of 2D arrays of NAs: one is able to detect molecules in the absorption region of the nitrile group, characterized by the stretching of the C≡N triple bond at around 2100 cm^{-1}; the second is capable of detecting molecules in the absorption region of the carbonyl group, characterized by the stretching of the C=O double bond at around 1700 cm^{-1}. We show a sensitivity of 600 nm/*RIU* at different wavelengths, with amounts of immobilized small molecules not higher than 0.7 fmoles, and a SEIRA enhancement factor of 48,000.

2. Materials and experimental methods

2.1. Simulations and design

The spectral response of the metasurface has been evaluated through numerical simulations by using COMSOL Multiphysics virtual environment. This allowed to design optimized 2D-arrays of gold NAs and fabricate high sensitivity SEIRA sensors for any fixed resonant wavelength λ_{res} [22]. In particular, we analyzed cross-shaped gold NAs because they ensure a metasurface polarization insensitive to the impinging EM radiation and an increase of about a factor two of the SEIRA sensitivity compared to that expected by employing rod shape NAs [22,23].

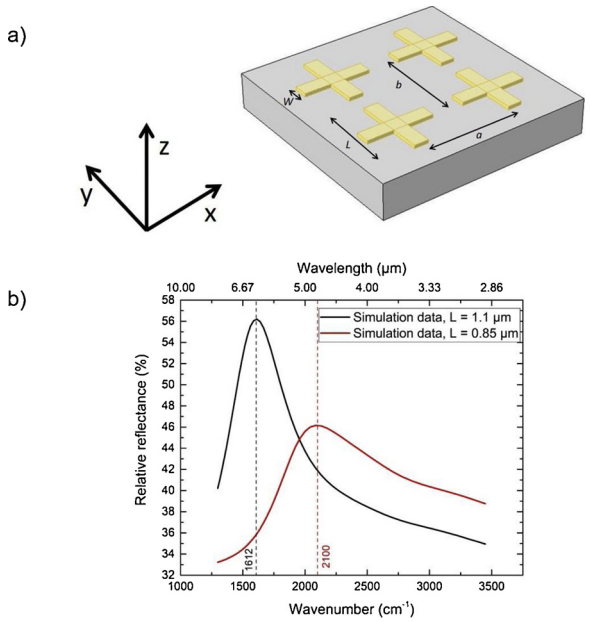

Fig. 1. Plasmonic NAs design and simulations. (a) Truncated view of the NAs 2D-array with the geometrical parameters for the cross-shaped NAs; (b) Finite Element Method – simulated reflectivity spectral response of resonant plasmonic NAs arrays centered at 1612 cm^{-1} and 2100 cm^{-1} obtained for NAs cross-length equal to $L = 1100$ nm (black curve) and $L = 850$ nm (red curve), respectively (For interpretation of the references to colour in this figure legend, the reader is referred to the web version of this article).

For the numerical simulations of the metasurface spectral behaviour, the unit cell of the 2D-array is composed by a single NA illuminated by an unpolarized EM plane wave propagating along the z-axis and impinging at normal incidence on the metasurface (Fig. 1). Starting from the unit cell, the NAs 2D-array was obtained by using periodic boundary conditions along the x- and y- axes (i.e. the metasurface plane) and the scattering boundary conditions along the z- axis. In Fig. 1**a**, L is the length of the cross arm, W the cross width and $a = b$ the distance between two adjacent crosses that defines the 2D-array periodicity. The NAs 2D-arrays are located on a silicon substrate (float zone Si) that is optically transparent in the middle and far infrared regions of the EM spectrum where the SEIRA experiments have been performed. As discussed above, the metasurface resonant wavelength depends on the values of the parameters indicated in Fig. 1, thus we fixed the 2D-array periodicity $a = b = 2$ μm and the cross-shape width $W = 0.2$ μm. Moreover, the NAs thickness was $t = 55$ nm (resulting from 5 nm of chromium and 50 nm of gold film deposition). With this design, the only 2D-array free parameter remains the cross-length L that was varied to center the metasurface resonance wavelength respect to the resonant absorption wavelength of the substances used for the SEIRA experiments. In particular, $L = 850$ nm was suggested by the simulations as the cross-length dimension needed to have a metasurface resonance at 2100 cm^{-1}, the wavelength that matches the vibration band of the nitrile group falling at around the same value. Under these conditions, the resulting metasurface peak reflectivity is equal to about 46% (see Fig. 1**b**, red curve). The cross-length $L = 1100$ nm was suggested to achieve the metasurface resonance centered at 1660 cm^{-1} needed to probe the vibrational band of the carbonyl group expected at about 1700 cm^{-1}. In this case, the metasurface maximum reflectivity is equal to 56% (see Fig. 1**b**, black curve). The metasurface was fabricated with NAs 2D arrays having these geometrical parameters. As defined in Ref. [22], the SEIRA gain is the ratio $\Delta R/\Delta R_0$ where ΔR and ΔR_0 are the changes of the reflectivity of the metasurface and of a flat unstructured metal layer calculated in presence and in absence of the adsorbed analyte for the maximum absorption coefficient centered at λ_{res}. Physically, the SEIRA gain depends on the electric field intensity distribution on the NA unit cell surface and, in particular, on its increase in the regions between the edges of the neighbouring adjacent crosses that strongly enhances the EM interaction with the substance adsorbed on the metasurface [22]. In Fig. 2 are reported the 2D plots of the spatial distribution of the electric field intensity on the NA unit cell area for the metasurface with the reflection resonance at 1660 cm^{-1}. Similar results are obtained for the metasurface with the reflection resonance at 2100 cm^{-1}. In particular, Fig. 2**a** shows the electric field intensity distribution taken at 20 nm above the NA unit cell surface that is located on the (x,y)-plane perpendicular to the z-direction of the EM radiation impinging on the metasurface. As expected the electric field distribution is greatly enhanced around the cross edges. The electric field intensity distribution on the xz-plane is reported in Fig. 2**b**. In this case we observe only the 50 nm NA cross section along the z-axis and the plot proves again that the increase of the electric field intensity is concentrated around the cross edges. Moreover, it is possible to observe that the regions yielding the increase of the electric field intensity as well as the corresponding maximum reached values, are different in the upper and lower part of the plane delimited by the unit cell of the NAs. This depends on the diverse differences of the permittivity occurring at the gold-vacuum (upper half-plane) and gold-silicon (lower half-plane)

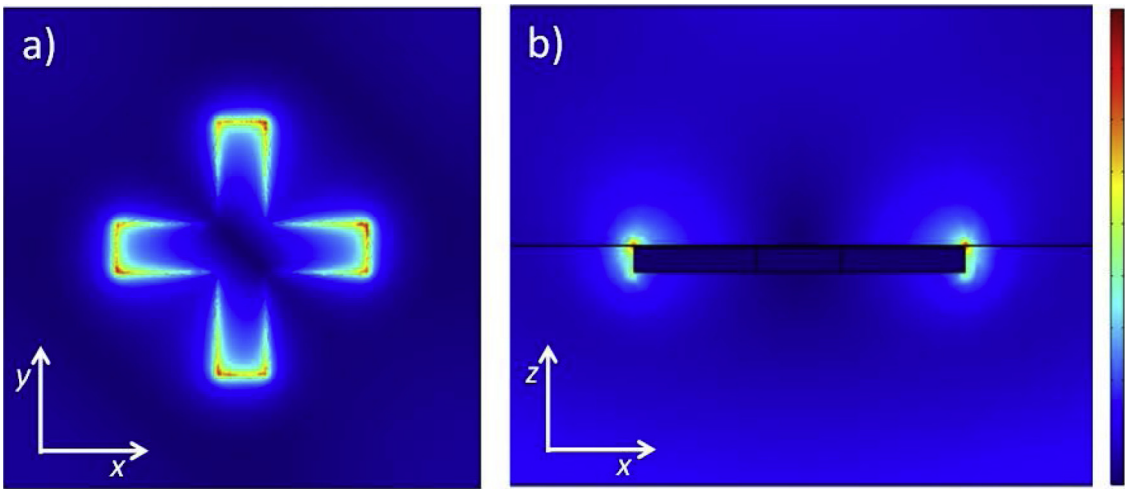

Fig. 2. 2D plots of the electric field intensity distribution on the NA unit cell. (a) Electric field intensity distribution taken at 20 nm above the NA unit cell surface on the (x,y)-plane perpendicular to the z-direction of the impinging EM radiation. (b) Electric field intensity distribution on the (x,z)-plane corresponding to the NA unit cell cross section view. Note that the cross dimensions are not in scale.

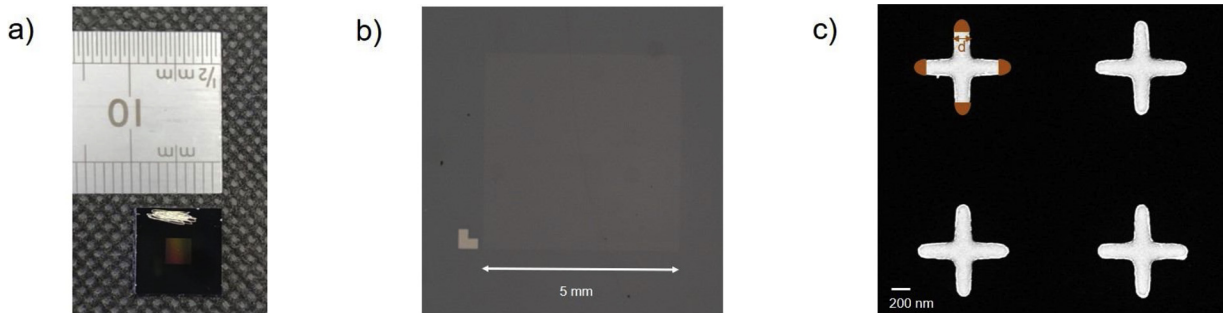

Fig. 3. SEIRA chips. (a) A macrophotograph of a 1 cm^2 chip containing a 3 × 3 mm^2 NAs array. (b) A micrograph of a 5 × 5 mm^2 array. (c) A scanning electron micrograph of NAs with L = 1100 nm and W = 190 nm with periodicity 2 μm; d = 200 nm.

interfaces.

2.2. Fabrication

We fabricated homogeneous NAs 2D-array on large areas as required for practical applications. The area coverage spans from 1 × 1 mm^2 to 5 × 5 mm^2, in order to be easily mounted on commercial FTIR instrument. The large area sample was fabricated by Electron Beam Lithography, by stitching up to 2500 writing field of size 100 × 100 μ m^2. With this write field size the stitching error is estimated to be 7 nm, enabling the fabrication of gold NAs with well-defined geometrical parameters. Fig. 3 shows a photograph of the whole device. Fig. 3**a** shows a macrograph of the whole chip of dimensions 10 × 10 mm^2, with a NAs array area coverage of 3 × 3 mm^2. Fig. 3**b** shows a micrograph of an NAs array with area coverage of 5 × 5 mm^2; Fig. 3**c** shows a scanning electron micrograph of single NAs with length L = 1100 nm, width W = 200 nm and a period of 2 μm. We used float-zone silicon wafer as substrate and designed a negative mask layer to be exposed on a layer of positive tone resist. After the development process we deposited a 5 nm chromium buffer layer and a 50 nm gold layer; the desired array was obtained via a lift-off process. The NAs fabricated are very robust and reusable. The array is very homogeneous and reproducible as confirmed by its infrared optical properties measured at different positions with distances of about 1 mm. Different devices produced with the same set of parameters show the same spectral feature of their resonance with a margin of error less than 5% as shown in **Figure S2** (see supplementary information (SI) document). We regenerated our gold metasurface covered by adsorbed thiols and polymers using liquid-phase hydrogen peroxide-mediated UV photo oxidation process [24] without observing any degradation of the performance (see **Figure S3**). All the details on the fabrication and regeneration process are reported in the paragraph **S.1** (SI).

2.3. Chemicals

To demonstrate the ability of the SEIRA chip to efficiently detect compounds absorbing at the expectede wavelengths, we designed and prepared some model compounds. Compound **I** containe on one end a thiol group for proper anchoring on the gold surface and on the other a nitrile group which resonates at about 2100 cm^{-1} the frequency at which the NAs with characteristic length L = 850 nm show the plasmon resonance. Compound **I** is a Pentinyl Cysteine Amide. The compound also contains two carbonyl groups that resonate at about 1650 cm^{-1}. Compound **II** was an azide-containing molecule specifically acetyl-lysine(ε-azide)-amide. Compound **II** that was used in a subsequent click chemistry reaction with the pentinyl moiety to transform the nitrile group into a triazolyl ring, thus removing the triple bond resonating at 2100 cm^{-1}. Compounds **I** and **II** were prepared following a standard methodology [25] on solid phase using 20 mg of Fluorenylmethyloxycarbonyl (Fmoc)- Rink Amide aminomethyl-polystyrene Resin (Rink Amide AM resin) for each compound, with a loading of 0.71 mmol/g. Compound **I** was obtained by condensation of pentinyl acid with a resin bound cysteine. Cysteine was introduced on the Rink Amide AM resin as Nα-(9- Fluorenylmethyloxycarbonyl)-S-trityl-L-cysteine (Fmoc-L-Cys (Trt) − OH). Condensation was performed using 1-[Bis(dimethylamino) methylene]-1*H*-1,2,3-triazolo[4,5-*b*]pyridinium 3-oxid hexafluorophosphate (HATU) and Sym-collidine. The Fmoc group was removed by a 10 min treatment with 20% piperidine in dimethylformamide (DMF). Compound II was obtained by coupling to the Rink Amide AM resin the Nα-(9- Fluorenylmethyloxycarbonyl)-ε-azido-L-lysine (Fmoc-L-Lys (N_3) − OH), removing the Fmoc group as described above and acetylating the free amino group with acetic anhydride at 30% in Dimethylformamide (DMF) in the presence of 5% N,*N*-Diisopropylethylamine (DIEA). Peptide cleavage from the resin and removal of the Trityl group from the cysteine side chain were carried out using Trifluoroacetic acid (TFA)/water (95:5) for 3 h. After resin removal by filtration, the cleavage mixture was diluted in water and lyophilized. Compounds were dissolved in water and residual organic solvents were extracted twice with diethyl ether. Analytical characterization of Compounds **I** and **II** by IR, nuclear magnetic resonance and mass spectrometry confirmed the identity of the molecules (see **Figure S4**, **S5**, **S6**). All the details on the synthesis and characterization of Compounds **I** and **II** are reported in the paragraph **S.2** (SI). Purity was higher than 99% as estimated by reverse phase high performance liquid chromatography (not shown).

Gold NAs were functionalized with a self-assembled monolayer of Compound **I**, by exposing the gold surface at a solution prepared at 10 pM in phosphate buffer pH 7.4 for 20 min. The whole array was covered with 200 μl of the compound solution. The reaction was repeated twice. Assuming a quantitative adsorption of the compound on the gold surface, no more than 0.7 fmoles of material were immobilized on the sensor, as described below. The click reaction was performed as reported in literature [26] exposing the gold surface conjugated with Compound **I** to a solution of Compound **II** at 1 μM in water/tert-butanol (2:1) in presence of copper(I) (concentration: 14 μM) and ascorbic acid (concentration: 13 μM) to promote the alkyne-azide cycloaddition. The functionalized layer was covered with 150 μl of the solution and allowed to react for one night. The reaction was repeated twice. Compound structures and a schematic of the click reaction are reported in Fig. 4.

To obtain a reference surface exposing carbonyl groups characterised by the absorption band at around 1700 cm^{-1}, we covered the gold NAs with characteristic length L = 1100 nm with a thin layer of Poly(Methyl MethAcrylate) (PMMA). We purchased the PMMA 1% in anisole w/v from Micro Chem (NANOTM PMMA) formulated with a molecular weight of 950,000 g/mol. We obtained 50 nm thin layer of PMMA via spin coating technique with a speed rotation of 2000 rpm for 60 s, baked at 180 °C for 180 s on a hot plate.

2.4. Infrared measurements

The reflectance spectra were acquired with a Perkin Elmer Spectrum

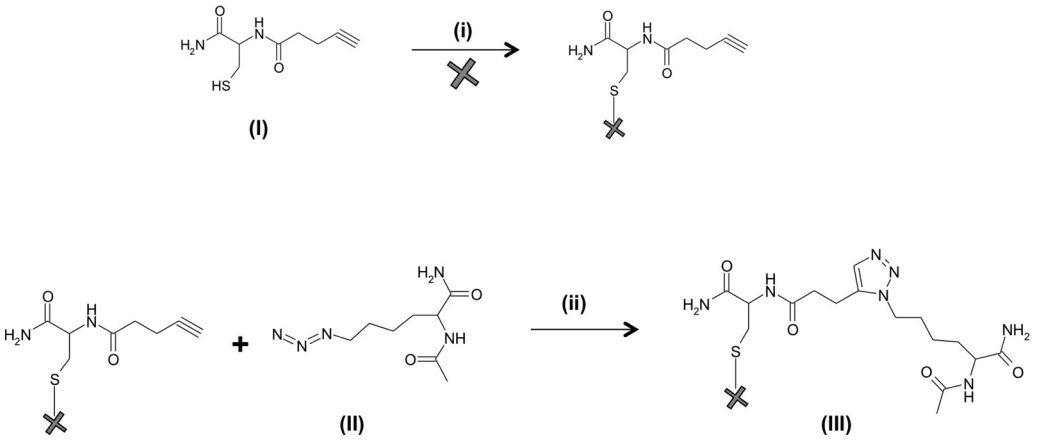

Fig. 4. Compounds used in this study. The gold surface is exemplified by a gray cross. Compound **I** is pentinyl-cysteineamide; compound **II** is acetyl-lysine (ε-azide)-amide. (i) 10 pM compound **I** in phosphate buffer pH 7.4, 200 µl, 20 min at room temperature (RT). (ii) 1 µM compound **II** in water/tBuOH (2:1), 14 µM Cu_2SO_4; 13 µM ascorbic acid, 150 µl, 2 h at RT. Compound **III** is 1-α-Acetyl-ε -lysinylamide-4-butylcarboxy-α-cysteinylamide triazole, linked to the gold surface through the thiol group.

One Fourier Transform Infrared (FTIR) spectrometer equipped with a Perkin Elmer Multiscope system infrared microscope and an MCT (mercury cadmium telluride) nitrogen cooled detector. The objective used for the measurements had a 10× optical or 15× infrared magnification. During the experiments, knife-edge apertures were set to form a measurement area ranging from 100 × 100 to 200 × 200 µm^2. A background spectrum was measured with an aperture of the same size on a flat unstructured gold layer with the same thickness of the NAs, deposited on the same substrate and utilized as a reference. The measurements were made at room temperature by collecting the signal in the spectral region between 4000 and 600 cm^{-1} using 128 scans with a spectral resolution of 4 cm^{-1} and 5 s as acquisition time for each spectrum.

3. Results and discussion

In order to demonstrate the ability of this specific design, i.e. gold cross-shaped NAs with specific sizes, to detect very low amounts (from femto down to attomoles) of molecules utilising the resonant SEIRA effect, we have chosen as probes two type of molecules, one type characterised by small molecular weight (Compound **I**, $C_8H_{13}N_2O_3S$ MW 200.06 g/mol and Compound **II**, $C_8H_{11}N_5O_2$ MW 215.14 g/mol), the other type by high molecular weight (PMMA MW 950,000 g/mol). In the first case the molecules bear a triple bond characterised by an absorption band at around 2100 cm^{-1} (Compound **I** at 2113 cm^{-1} due to the vibrational mode stretching ν((R-C≡C-H)) and Compound **II** at 2097 cm^{-1} due to the vibrational mode stretching ν(-N_3) as shown in **figure S5 A–B** in the SI). In the second case, the carbonyl groups of PMMA methyl acrylate are characterised by the absorption band at around 1700 cm^{-1} (1720 cm^{-1} due to the vibrational mode stretching of ν (COOCH3)).

Because of the resonant nature of the molecule-plasmon coupling, the enhanced vibrational signal strengths strongly depend on the plasmonic resonance frequency with respect to the vibrational one. To maximize this effect of increasing the SEIRA performance, a tailored and optimized design of NAs resonance is required. The ratio of absorption is determined by the plasmonic material while the scattering cross-section and the near field by the NAs geometry, which both impact the SEIRA enhancement. Typical materials used for resonant SEIRA include metals, e.g. Au, Al or Ag. Gold combines several advantages. Among the others, its dielectric function follows nearly perfect Drude-type behaviour in the infrared spectral range, leading to a sharp plasmonic resonance. In addition, gold is stable under ambient conditions, biocompatible and shows robust self-assembled monolayers through thiol–gold interaction. Therefore it is a promising material for biomedical applications. In the cross-shaped NAs we describe here, the plasmon resonance frequency can be tuned to the desired value of vibrational band by simply varying the NA length (which is inversely proportional to the value of the plasmon resonance frequency λ_{res}^{-1}). Following our simulation study, we fabricated NAs having length L = 850 nm to match the band at around 2100 cm^{-1} (see Fig. 1**b** red curve) and NAs having length L = 1100 nm to match the band at around 1700 cm^{-1} (see Fig. 1**b** black curve). In both cases the width W and periodicity a of the NAs array was fixed at W = 200 nm and a = 2000 nm.

Fig. 5**a** shows the comparison between measured and simulated reflection spectra of the NAs arrays tuned for the coupling to the triple bond vibrational band before molecule adsorption. A plasmonic resonance peaked at a wavenumber of 2099 cm^{-1} with a relative reflectance of 45% is present. Fig. 5**b** shows the comparison between measured and simulated reflection spectra of the NAs arrays tuned for the coupling to the double bond vibrational band before molecule adsorption. A plasmonic resonance peaked at a wavenumber of 1666 cm^{-1} with a relative reflectance of 56% is present. The positions of the peaks resonances are well fitted with the simulated model discussed above, confirming the model as a useful guide for the design of NAs arrays with specific resonance peaks. However the small discrepancy present in the figure is due to the difference between the real geometry of the fabricated nanostructures and the ideal design (see Fig. 3c) since during the electron beam fabrication procedure the proximity effect makes very difficult to produce sharp edges.

FTIR spectra were investigated before and after Compound **I** adsorption and after the click reaction with Compound **II** on the surface of the gold NAs arrays with L = 850 nm.

After the verification of the resonance properties, gold NAs were functionalized with a self-assembled monolayer of Compound **I**. Fig. 6 shows SEIRA spectra of a 1 × 1 mm^2 area coverage of a NAs array before and after adsorption of Compound **I** and after its conversion into 1-α-Acetyl-ε-lysinylamide-4-butylcarboxy-α-cysteinylamide triazole (compound **III**), where the C≡N group, following the click reaction is incorporated into a triazole ring, losing the triple bond feature.

The amount of Compound **I** detected in a single measure was estimated as follows: we determined the number of gold atoms exposed to the light beam on the outer surface of each NAs during the measurement and assumed that every single gold atom was able to capture one single molecule of Compound **I**. The outer surface of each NA with length of 850 nm is 5.3 × 10^5 nm^2. Considering an area coverage exposed to the light of 100 × 100 µ m^2 and a gold effective area of a single atom to be about 3.5 × 10^{-1} nm^2, we have about 4 × 10^9 exposed gold atoms, that means 0.7 fmoles of compound **I** (for an area coverage of 200 × 200 µ m^2 about 2.5 fmoles). Assuming a quantitative complexation of gold by the thiol groups of Compound I and a quantitative conversion of its alkyne group to the triazole ring of Compound III, we can infer that the maximum amount of both Compound I and of Compound III that can be detected in a single measure is not higher than 0.7 fmoles. After derivatization with Compound **I**, the plasmonic

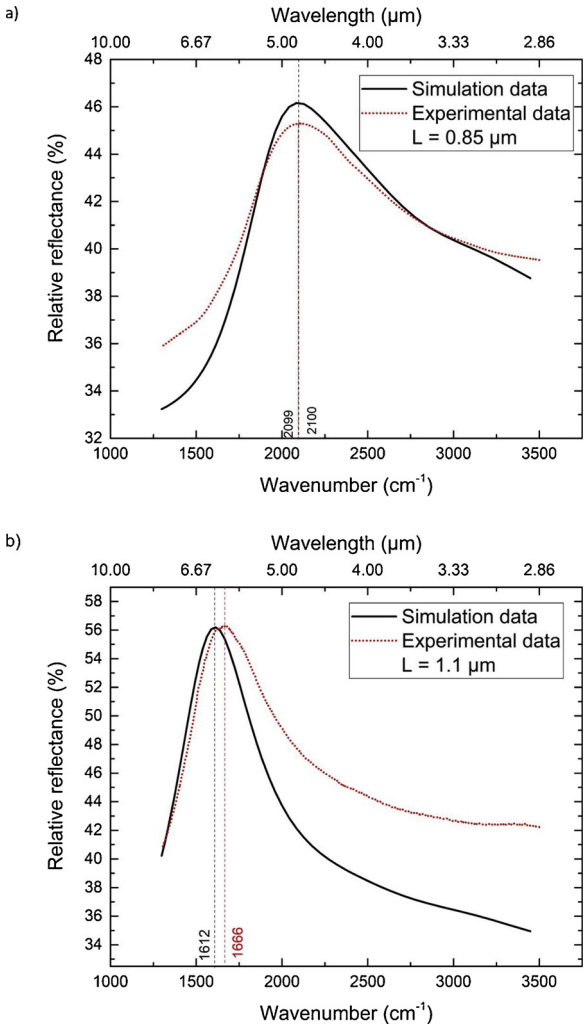

Fig. 5. Reflectance FTIR spectra. Comparison of simulated and experimental reflectance curve for naked NAs arrays (no compounds adsorbed), with a fixed period of 2 μm and NAs width of $W = 200$ nm and different NAs length: (a) $L = 850$ nm; (b) $L = 1100$ nm.

resonance peak is red shifted of 100 cm^{-1}. This shift originates from the polarizability change of the NAs surrounding medium caused by the adsorbed compound. This shift is the base of localized surface plasmon resonance (LSPR) sensing [12] and originates from the confined plasmonic near-field, which at visible and near infrared wavelengths is highly sensitive to the change in refractive index of its surrounding medium. Reported sensitivity for LSPR sensors are $\sim 2x10^2$ nm/*RIU* [27,28]. Although less performing than Surface Plasmon Polaritons (SPP), LSPR-based sensors can perform well in some instances, particularly for the detection of small number of biomolecules with small molecular weight < 500 g/mol (Compound **I** has a MW of 200 g/mol). The difference between the refractive index of the air and of Compound **I** is 0.42 [29] and we found a sensitivity of 600 nm/*RIU*. This value is in accordance with the values reported for similar molecular systems [27,28].

Although we were able to detect Compound **I** at as low as 0.7 fmoles or less, the resonant effect did not show up. SEIRA resonant effect did not appear even if the NAs are properly designed and fabricated. This may be due to different reasons, like quantum effects [30] and/or damping and surface effects originating from impurities that hinder adsorption of the molecules of interest at the site of the plasmonic enhancement [31]. In our case, the main reasons can be attributed to the small molecular weight of the molecule. The experiment was

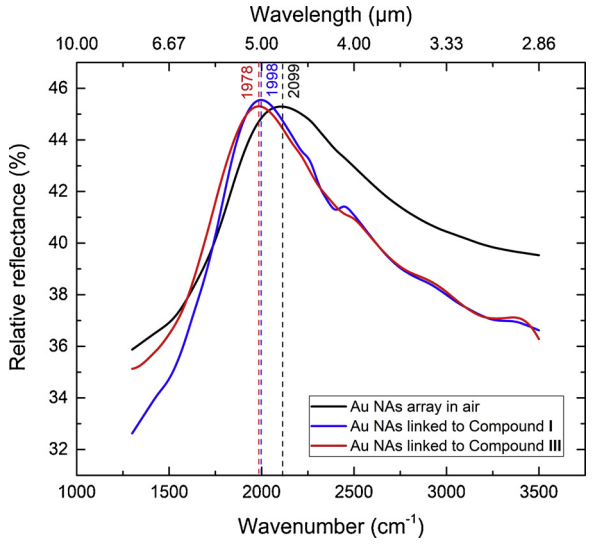

Fig. 6. Non-resonant SEIRA spectra. Reflectance curve of gold NAs array in air: the black curve is referred to naked NAs arrays; the blue curve is referred to the NAs array linked to Compound **I**; the blue curve is referred to the NAs array linked to Compound **III** (For interpretation of the references to colour in this figure legend, the reader is referred to the web version of this article).

planned in such a way that the resonant effect of the stretching of C≡N through to the conversion of the triple bond to the triazole function caused by a click chemistry reaction could be controlled and dumped. Although the resonant effect did not occur we determined the sensitivity of the sensor to the modified layer of molecules, i.e. the layer of Compound **I**, through the resonance shift. Indeed, following the click reaction and formation of the triazole moiety in Compound **III**, we observed a further 20 cm^{-1} red shift (Fig. 6, red curve) compared to the Compound **I** resonance (Fig. 6, blue curve).

To test the SEIRA resonant effect at wavenumbers where the C═O groups are detected, we deposited a thin layer of high molecular weight PMMA (about 950,000 g/mol) that contains a high density of repeating C═O units. A thickness value of 50 nm was chosen to fully cover the NAs [32]. Fig. 7 presents SEIRA spectra recorded on a 5 × 5 mm^2 area of NAs arrays, illuminating a 200 × 200 μ m^2 area, before and after the PMMA deposition. The black curve in Fig. 7 shows the characteristic resonance of the NAs array in air peaked at 1666 nm^{-1}. After PMMA deposition, the peak position of the plasmonic resonance was red-shifted by 66 cm^{-1}. The difference between refractive index of the air and PMMA is 0.49 [33] and we found a sensitivity of 505 nm/RIU.

Resonant coupling between the NAs plasmonic resonance and the stretching vibration of the carbonyl groups of PMMA methyl acrylate ν(COOCH3) is found in our spectra at 1720 cm^{-1} in good agreement with data reported for PMMA. The good match of the NAs resonance with the C═O stretching vibration band is crucial for the appearance of the vibrational signal. The signal intensity, calculated as difference between maximum and minimum reflectance at the vibrational feature, reaches a value of about 2%. To quantify the sensitivity of resonant SEIRA effects we adopted the following enhancement factor (EF) parameter, which correlates the enhanced signal strengths to standard IR reflection measurements [11,34]:

$$EF = \frac{\Delta R}{\Delta R_0} \bullet \frac{A_0}{A_{SEIRA}} \quad (1)$$

where ΔR is the difference of the reflectance value of the NAs array without the PMMA layer (Fig. 7, black curve) and with the PMMA layer taken in correspondence of the stretching vibration of the carbonyl group of methyl acrylate ν(COOCH3) at 1720 cm^{-1} (Fig. 7, red curve at the minimum of the SEIRA resonant peak). ΔR turns out to be equal to 7%. In the same way ΔR_0 is the difference of the reflectance value of a

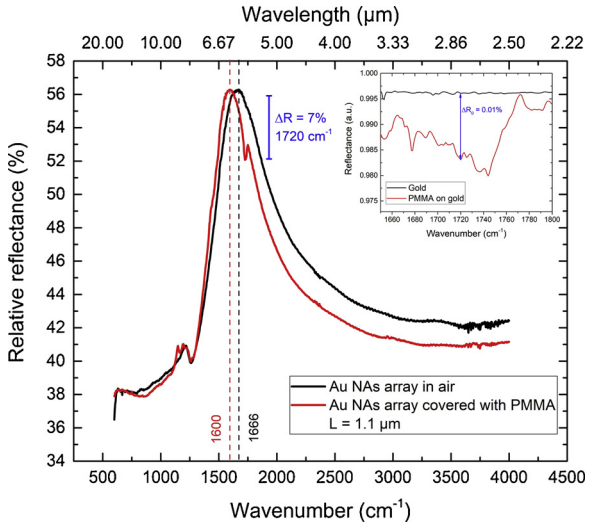

Fig. 7. Resonant SEIRA spectra. Reflectance curve of the gold NAs array in air: the black curve is referred to naked NAs arrays and red curve is referred to the NAs array covered with a 50 nm PMMA layer. Inset: spectrum of 50 nm flat unstructured gold layer; black curve shows the reflectance in air, red curve shows the reflectance with a 50 nm PMMA layer deposited on it (For interpretation of the references to colour in this figure legend, the reader is referred to the web version of this article).

flat unstructured gold layer with the same thickness of the NAs, deposited on the same substrate, acquired in the same conditions utilised for NAs array, without the PMMA layer (Fig. 7, inset black curve) and with the PMMA layer at 1720 cm^{-1} (Fig. 7 inset red curve). ΔR_0 turns out to be equal to 0.01%. The factor $\Delta R/\Delta R_0$ result to be $\approx$ 700.

For the determination of the geometrical parameter, A_0 is the area of the NAs exposed to the light corresponding in this case to 4×10^{10} nm^2 and A_{SEIRA} is the effective area of NAs on which the field is located. As reported in literature [15,35] and as seen in Fig. 2**a** the field is mainly located on the tips of the cross shaped NAs, therefore we evaluate the active area for each NA as the sum of four semi-circles with a 200 nm diameter (schematic in Fig. 1b) then multiplied for the number of exposed NAs. A_{SEIRA} turns out to be 2π x10^8 nm^2. The geometrical factor A_0/A_{SEIRA} is equal to 64, therefore we have an enhancement factor of 44,800.

Typical enhancement factors found in other studies range from 10^3 to 10^5 depending on the antenna shape, material, and arrangement. The value found for the EF parameter confirms the goodness of our devices and of the model used for their design [22]. Moreover, our device shows the capability to perform both refractive index sensing and surface-enhanced infrared absorption spectroscopy.

4. Conclusion

In conclusion, we have experimentally demonstrated that high-density arrays of gold cross-shaped NAs are very suitable for both sensitive surface enhanced infrared absorption spectroscopy and refractive index sensing. The gold cross-shaped NAs support localized surface plasmon polaritons; the resonance peak of the NAs array has been tuned by varying one geometrical parameter, i.e. the length of NA. In presence of a layer of PMMA that contains repeated carbonyl groups, the SEIRA enhancement has been found to be as high as 48,000 relative to the absorption peak at 1720 cm^{-1}, arising from the stretching vibration of the carbonyl group of the PMMA methyl acrylate ν(COOCH3). For small molecules with a size well below 500 g/mol (Compound **I** MW 200 g/mol), a sensitivity of 600 nm / RIU has been found for amounts of immobilized compound as low as 0.7 fmoles or less.

The manufactured devices have shown an excellent reproducibility and an excellent robustness. In fact, they have been recycled using a liquid-phase hydrogen peroxide-mediated UV photo oxidation process for regenerating the naked gold surface.

By increasing the NA length and hence decreasing its resonance frequency, the plasmonic near-field intensity increases [36], therefore a higher SEIRA enhancement is expected. This observation also suggests a huge potential for the use of plasmonic enhancement in THz spectroscopy [37]. The SEIRA enhancement may be further improved by a careful design to reduce non-radiative plasmonic losses given by the NAs materials [38] and of the radiative plasmonic losses provided by the specific NAs shapes and arrangements [39]. Such optimized nanoantennas are likely to serve as substrates for surface-enhanced infrared spectroscopy with very high sensitivity, with the capability for label-free and non-destructive material identification and for monitoring at qualitative level chemical transformations occurring at the sensor surface. Moreover, combinations of resonant SEIRA with refractive index sensing and other field-enhanced techniques, can lead to the design of nanoscale sensing platforms providing complementary chemical information and quantitative assessment of known analytes following proper calibrations with suitable standards. Finally, SEIRA NAs can be easily integrated with micrometre-sized channels and be suitable for the high sensitivity, real time analysis of IR emitting samples, in matrices where IR spectroscopy is severely limited due to absorption bands of liquid water.

Acknowledgements

The work has been supported by MIUR - project PRIN2015783N45. Authors acknowledge Maurizio Amendola for his technical advice and support for mass spectrometry.

Appendix A. Supplementary data

Supplementary material related to this article can be found, in the online version, at doi:https://doi.org/10.1016/j.snb.2019.02.014.

References

[1] J. Chalmers, P.R. Griffiths, Handbook of Vibrational Spectroscopy, John Wiley & Sons, UK, 2003.
[2] B.H. Stuart, Spectral Analysis, John Wiley & Sons, UK, 2005.
[3] P.R. Griffiths, J.A. de Haseth, Fourier Transform Infrared Spectrometry, John Wiley & Sons, UK, 2007.
[4] K.A. Willets, R.P. Van Duyne, Localized surface plasmon resonance spectroscopy and sensing, Annu. Rev. Phys. Chem. 58 (2007) 267–297.
[5] J. Homola, S.S. Yee, G. Gauglitz, Surface plasmon resonance sensors: review, Sens. Actuators B Chem. 54 (1999) 3–5.
[6] J. Homola, Present and future of surface plasmon resonance biosensors, Anal. Bioanal. Chem. 377 (2003) 528–539.
[7] A.G. Brolo, Plasmonics for future biosensors, Nat. Phot. 6 (2012) 709–713.
[8] E. Aslan, S. Kaya, E. Aslan, S. Korkmaz, O.G. Saracoglu, M. Turkmen, Polarization insensitive plasmonic perfect absorber with coupled antisymmetric nanorod array, Sens. Actuators B Chem. 243 (2017) 617–625.
[9] M. Janneh, A. De Marcellis, E. Palange, A.T. Tenggara, D. Byun, Design of a metasurface-based dual-band Terahertz perfect absorber with very high Q-factors for sensing applications, Opt. Comm. 416 (2018) 152–159.
[10] W.J. Padilla, M.T. Aronsson, C. Highstrete, M. Lee, A.J. Taylor, R.D. Averitt, Electrically resonant terahertz metamaterials: theoretical and experimental investigations, Phys. Rev. B 75 (2007) 041102-1–041102-4.
[11] F. Neubrech, C. Huck, K. Weber, A. Pucci, H. Giessen, Surface-enhanced infrared spectroscopy using resonant nanoantennas, Chem. Rev. 117 (2017) 5110–5145.
[12] R. Adato, S. Aksu, H. Altug, Engineering mid-infrared nanoantennas for surface enhanced infrared absorption spectroscopy, Mater. Today 18 (2015) 436–446.
[13] F. Le, D.W. Brandl, Y.A. Urzhumov, H. Wang, J. Kundu, N.J. Halas, J. Aizpurua, P. Nordlander, Metallic nanoparticle arrays: a common substrate for both surface-enhanced raman scattering and surface-enhanced infrared absorption, ACS Nano 2 (2008) 707–718.
[14] L. Novotny, Effective wavelength scaling for optical antennas, Phys. Rev. Lett. 98 (2007) 266802.
[15] F. Neubrech, A. Pucci, T.W. Cornelius, S. Karim, A. Garcia-Etxarri, J. Aizpurua, Resonant plasmonic and vibrational coupling in a tailored nanoantenna for infrared detection, Phys. Rev. Lett. 101 (2008) 157403.
[16] R. Adato, A.A. Yanik, H. Altug, On chip plasmonic monopole nano-antennas and circuits, Nano Lett. 11 (2011) 5219–5226.

[17] R. Bukasov, J.S. Shumaker-Parry, Silver nanocrescents with infrared plasmonic properties as tunable substrates for surface enhanced infrared absorption spectroscopy, Anal. Chem. 81 (2009) 4531–4535.
[18] J. Paul, R.M. De La Rue, N.P. Johnson, Gold asymmetric-Split ring resonators (A-SRRs) for proteins sensing, Proc. SPIE, SPIE Phototonics Europe: Metamaterials X (2016) 98831C.
[19] D. Dregely, F. Neubrech, H. Duan, R. Vogelgesang, H. Giessen, Vibrational near-field mapping of planar and buried three-dimensional plasmonic nanostructures, Nat. Commun. 4 (2013) 2237.
[20] F.J. Rodríguez-Fortuño, M. Martínez-Marco, B. Tomás-Navarro, R. Ortuño, J. Martí, A. Martínez, P.J. Rodríguez-Cantó, Highly-sensitive chemical detection in the infrared regime using plasmonic gold nanocrosses, Appl. Phys. Lett. 98 (2011) 133118.
[21] L. Businaro, O. Limaj, V. Giliberti, M. Ortolani, A. Di Gaspare, G. Grenci, G. Ciasca, A. erardino, A. de Ninno, S. Lupi, Mid-infrared nanoantenna arrays on silicon and CaF2 substrates for sensing applications, Microelectron. Eng. 97 (2012) 197–200.
[22] A. De Marcellis, E. Palange, M. Janneh, C. Rizza, A. Ciattoni, S. Mengali, Design optimisation of plasmonic metasurfaces for mid-infrared high-sensitivity chemical sensing, Plasmonics 12 (2017) 293–298.
[23] S. Bagheri, K. Weber, T. Gissibl, T. Weiss, F. Neubrech, H. Giessen, Fabrication of square-centimeter plasmonic nanoantenna arrays by femtosecond direct laser writing lithography: effects of collective excitations on SEIRA enhancement, ACS Photonics 2 (2015) 779–786.
[24] B.N. Johnson, R. Mutharasan, Regeneration of gold surfaces covered by adsorbed thiols and proteins using liquid-phase hydrogen peroxide-mediated UVPhotooxidation, J. Phys. Chem. C 117 (2013) 1335–1341.
[25] A. Caporale, N. Doti, A. Sandomenico, M. Ruvo, Evaluation of combined use of Oxyma and HATU in aggregating peptide sequences, J. Pept. Sci. 23 (2017) 272–281.
[26] V. Castro, H. Rodriguez, F. Albericio, CuAAC: an efficient click chemistry reaction on solid phase, ACS Comb. Sci. 18 (2016) 1–14.
[27] H. Chen, X. Kou, Z. Yang, W. Ni, J. Wang, Shape- and size-dependent refractive index sensitivity of gold nanoparticles, Langmuir 24 (2008) 5233–5237.
[28] T. Sannomiya, J. Voros, Single plasmonic nanoparticles for biosensing, Trends Biotechnol. 29 (2011) 343–351.
[29] F. Koohyar, A.A. Rostami, M.J. Chaichi, F. Kiani, Refractive Indices, Viscosities, and Densities for L-Cysteine, J. Sol. Chem. 40 (2011) 1361–1370.
[30] J. Zuloaga, E. Prodan, P. Nordlander, Quantum plasmonics: optical properties and tunability of metallic nanorods, ACS Nano 4 (2010) 5269–5276.
[31] J. Bochterle, F. Neubrech, T. Nagao, A. Pucci, Angstrom-scale distance dependence of antenna-enhanced vibrational signals, ACS Nano 6 (2012) 10917–10923.
[32] F. Neubrech, S. Beck, T. Glaser, M. Hentschel, H. Giessen, A. Pucci, Spatial extent of plasmonic enhancement of vibrational signals in the infrared, ACS Nano 8 (2014) 6250–6258.
[33] MicroChem Corp. http://microchem.com/pdf/PMMA_Data_Sheet.pdf.
[34] C. D'Andrea, J. Bochterle, A. Toma, C. Huck, F. Neubrech, E. Messina, B. Fazio, O.M. Marag, E. Di Fabrizio, M.L. De La Chapelle, P.C. Gucciardi, A. Pucci, Optical nanoantennas for multiband surface-enhanced infrared and raman spectroscopy, ACS Nano 7 (2013) 3522–3531.
[35] D. Dregely, F. Neubrech, H. Duan, R. Vogelgesang, H. Giessen, Vibrational near-field mapping of planar and buried three-dimensional plasmonic nanostructures, Nat. Commun. 4 (2013) 2237.
[36] R. Bukasov, T.A. Ali, P. Nordlander, J.S. Shumaker-Parry, Probing the plasmonic near-field of gold nanocrescent antennas, ACS Nano 4 (2010) 6639–6650.
[37] K.V. Sreekanth, Y. Alapan, M. ElKabbash, E. Ilker, M. Hinczewski, U.A. Gurkan, A. De Luca, G. Strangi, Extreme sensitivity biosensing platform based on hyperbolic metamaterials, Nat. Mater. 15 (2016) 621–627.
[38] M. Abb, Y. Wang, N. Papasimakis, C.H. de Groot, O.L. Muskens, Surface-enhanced infrared spectroscopy using metal oxide plasmonic antenna arrays, Nano Lett. 14 (2014) 346–352.
[39] D. Yoo, D.A. Mohr, F. Vidal-Codina, A. John-Herpin, M. Jo, S. Kim, J. Matson, J.D. Caldwell, H. Jeon, N. Nguyen, L. Martin-Moreno, J. Peraire, H. Altug, S.H. Oh, High-contrast infrared absorption spectroscopy via mass-produced coaxial zero-mode resonators with Sub-10 nm gaps, Nano Lett. 18 (2018) 1930–1936.